Shell-model study of boron, carbon, nitrogen, and oxygen isotopes with a monopole-based universal interaction

Cenxi Yuan,[1,2,*] Toshio Suzuki,[3,4,†] Takaharu Otsuka,[2,5,6,‡] Furong Xu,[1,7,§] and Naofumi Tsunoda[2]

[1]*State Key Laboratory of Nuclear Physics and Technology, School of Physics, Peking University, Beijing 100871, China*

[2]*Department of Physics, University of Tokyo, Hongo, Bunkyo-ku, Tokyo 113-0033, Japan*

[3]*Department of Physics, College of Humanities and Sciences, Nihon University, Sakurajosui 3, Setagaya-ku, Tokyo 156-8550, Japan*

[4]*National Astronomical Observatory of Japan, Mitaka, Tokyo 181-8588, Japan*

[5]*Center for Nuclear Study, University of Tokyo, Hongo, Bunkyo-ku, Tokyo 113-0033, Japan*

[6]*National Superconducting Cyclotron Laboratory, Michigan State University, East Lansing, Michigan, 48824, USA*

[7]*Center for Theoretical Nuclear Physics, National Laboratory for Heavy Ion Physics, Lanzhou 730000, China*

(Received 17 April 2012; revised manuscript received 7 June 2012; published 22 June 2012)

We study boron, carbon, nitrogen, and oxygen isotopes with a newly constructed shell-model Hamiltonian developed from a monopole-based universal interaction (V_{MU}). The present Hamiltonian can reproduce well the ground-state energies, energy levels, electric quadrupole properties, and spin properties of these nuclei in full psd model space including $(0-3)\hbar\omega$ excitations. Especially, it correctly describes the drip lines of carbon and oxygen isotopes and the spins of the ground states of ^{10}B and ^{18}N while some former interactions such as WBP and WBT fail. We point out that the inclusion of $2\hbar\omega$ excitations is important in reproducing some of these properties. In the present $(0+2)\hbar\omega$ calculations small but constant $E2$ effective charges appear to work quite well. As the inclusion of the $2\hbar\omega$ model space makes a rather minor change, this seems to be related to the smallness of the ^{4}He core. Similarly, the spin g factors are very close to free values. The applicability of tensor and spin-orbit forces in free space, which are taken in the present Hamiltonian, is examined in shell-model calculations.

DOI: 10.1103/PhysRevC.85.064324 PACS number(s): 21.60.Cs, 21.30.Fe, 23.20.−g, 27.20.+n

I. INTRODUCTION

The existence of the unexpected doubly magic nucleus ^{24}O shows the exotic property of drip-line nuclei; that is, the change of magic numbers far from the stability [1]. One of the aims of theoretical works on nuclear structure is to describe both stable nuclei and nuclei far from the stability in a unified framework. In shell-model studies, for many existing conventional interactions, it is difficult to reproduce simultaneously the drip lines of carbon and oxygen isotopes as well as some other properties such as the energies of 2_1^+ states and $B(E2)$. From a microscopic study, the inclusion of effects of the three-body force is important in describing the drip line of oxygen isotopes [2]. It is urgent to construct new shell-model interactions applicable from the β-stability line to the drip lines.

The realistic nucleon-nucleon (NN) interactions need to be renormalized when applied to shell-model calculations because of the short-range correlation and in-medium effect [3]. The NN interaction is composed of three components: the central force, spin-orbit force, and tensor force. Recent studies show that the monopole components of the tensor force barely change after renormalization and that the multipole components also change little [4,5]. Based on these studies, a monopole-based universal interaction (V_{MU}) including the bare $\pi+\rho$ tensor force is introduced to describe the shell evolution [4]. As this V_{MU} is constructed based on monopole properties, it requires examination as to whether V_{MU} can be used or not in actual shell-model calculations. In this paper we try to apply the V_{MU} to shell-model calculations in psd model space.

In the psd region, several effective interactions have been introduced in shell-model calculations, such as PSDMK [6], the Warburton-Brown WBT [7] and WBP [7], and SFO [8]. The PSDMK, WBT, and WBP interactions are all constructed in $(0-1)\hbar\omega$ model space, which means that $0-1$ nucleons are allowed to be excited from p shell to sd shell. The mixing between $(0-1)\hbar\omega$ states and $(2-3)\hbar\omega$ states is not considered in the fitting of the interaction. SFO, which includes the $(2-3)\hbar\omega$ states, concentrates mostly on the spin properties such as magnetic moments and Gamow-Teller transitions. Up to now, the $\langle pp|V|sdsd\rangle$ matrix elements, which represent the interaction between $(0-1)\hbar\omega$ states and $(2-3)\hbar\omega$ states, have not been well studied. In Ref. [9], the tensor part of the $\langle psd|V|psd\rangle$ matrix elements is taken to be that of the $\pi+\rho$ meson exchange potential and the spin properties of C isotopes are studied. Recently, the study of the microscopic derivation of the effective interaction for the shell model in two major shells has begun [10]. It would be interesting to apply the results to future shell-model calculations.

In this paper we try to construct the effective interaction in psd space based on V_{MU} to describe ground-state energies, energy levels, electric quadrupole properties, and spin properties. The $\langle psd|V|psd\rangle$ and $\langle pp|V|sdsd\rangle$ matrix elements are obtained based on V_{MU} while phenomenological effective

*cxyuan@pku.edu.cn
†suzuki@phys.chs.nihon-u.ac.jp
‡otsuka@phys.s.u-tokyo.ac.jp
§frxu@pku.edu.cn

interactions are used for the p-shell and sd-shell parts to maintain the good description of the phenomenology by these interactions. Microscopic interactions have been obtained based on the G-matrix method with medium modification [11], the similarity renormalization group (SRG) method [12] and the coupled-cluster method [13]. While they produce interesting results, fully microscopic calculations have not been successful, as far as a good agreement to experiment is concerned. We restrict ourselves here to a more phenomenological approach based on V_{MU} to study the spectroscopic properties of the nuclei to be discussed.

In the next section, we introduce the Hamiltonian. Coulomb correction and center-of-mass correction are discussed in Secs. III and IV, respectively. In Sec. V, we discuss the ground-state energies and energy levels. We present the results of electric quadrupole properties and spin properties in Secs. VI and VII, respectively. A summary is given in Sec. VIII.

II. HAMILTONIAN

The present Hamiltonian is developed from V_{MU}, SFO, and SDPF-M [14]. The two-body matrix elements (TBME) are constructed as follows: $\langle pp|V|pp\rangle$ from SFO, $\langle sdsd|V|sdsd\rangle$ from SDPF-M, $\langle psd|V|psd\rangle$, and $\langle pp|V|sdsd\rangle$ from V_{MU} plus the spin-orbit force. In the $\langle pp|V|pp\rangle$ matrix elements, we reduce the strength of the monopole term $\langle p_{1/2}p_{3/2}|V|p_{1/2}p_{3/2}\rangle_{T=0}$ by 0.5 MeV from SFO. This will improve the description of the ground-state energies of these nuclei. The $\langle sdsd|V|sdsd\rangle$ matrix elements in the present Hamiltonian are the same as SDPF-M. In earlier interactions, such as WBP and WBT, the matrix elements $\langle pp|V|sdsd\rangle$ are not considered in the fitting procedure. The strength of the interaction in $\langle pp|V|sdsd\rangle$ in WBP and WBT is the same as in $\langle psd|V|psd\rangle$ in WBP. In the present interaction, strengths of these two parts of the interaction are not taken to be the same. V_{MU} includes a Gaussian-type central force and a $\pi+\rho$ tensor force. We use an M3Y [15] force for the spin-orbit force. We keep the spin-orbit and tensor forces unchanged. The form of the interactions in the matrix elements of $\langle psd|V|psd\rangle$ and $\langle pp|V|sdsd\rangle$ is as follows:

$$V = V_{\text{central}} + V_{\text{spin-orbit}}(\text{M3Y}) + V_{\text{tensor}}(\pi+\rho), \quad (1)$$

with V_{central} being

$$V_{\text{central}} = \sum_{S,T} f_{S,T} P_{S,T} \exp[-(r/\mu)^2], \quad (2)$$

where S (T) means spin (isospin) and P_S (P_T) is the projection operator on the S (T) channel. r and μ are the distance between two nucleons and the Gaussian parameter, respectively. f_{ST} is the strength of the central force. In the original V_{MU}, $f_{0,0} = f_{1,0} = -166$ MeV, $f_{0,1} = 0.6 f_{0,0}$, and $f_{1,1} = 0.8 f_{0,0}$ [4]. In the present study, we reduce the central force in the $\langle psd|V|psd\rangle$ and $\langle pp|V|sdsd\rangle$ matrix elements by factors of 0.85 and 0.55, respectively, from the original V_{MU}. The final interaction in the $\langle psd|V|psd\rangle$ ($\langle pp|V|sdsd\rangle$) matrix elements is

$$V = 0.85(0.55)V_{\text{central}} + V_{\text{spin-orbit}}(\text{M3Y}) + V_{\text{tensor}}(\pi+\rho). \quad (3)$$

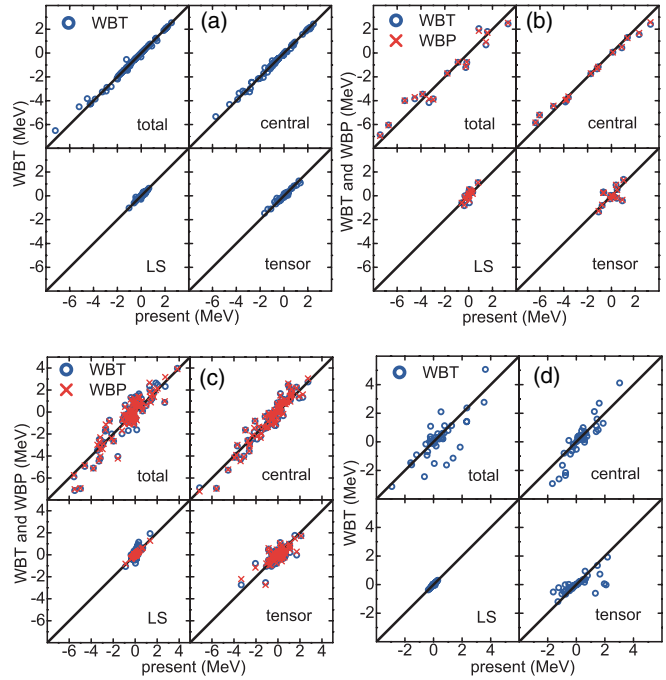

FIG. 1. (Color online) Total TBME, TBME of central force, spin-orbit force, and tensor force in each part of interaction: (a) $\langle sdsd|V|sdsd\rangle$, (b) $\langle pp|V|pp\rangle$, (c) $\langle psd|V|psd\rangle$, and (d) $\langle pp|V|sdsd\rangle$.

Notice that the spin-orbit force and the tensor force are kept unchanged. The TBME are calculated with harmonic oscillator parameter $\hbar\omega = 45A^{-1/3} - 25A^{-2/3}$ where $A = 18$ which is the average mass number of the investigated nuclei from ^{10}B to ^{26}O. The sd-shell single-particle energies (SPEs) in SDPF-M are $\epsilon_{d_{5/2}} = -3.95$ MeV, $\epsilon_{d_{3/2}} = 1.65$ MeV, and $\epsilon_{s_{1/2}} = -3.16$ MeV, which takes ^{16}O as the core [14]. In the present shell-model calculations, ^{4}He is chosen as the core, thus the sd-shell SPEs in the present Hamiltonian should be adjusted to give the same one-particle excitation energies for ^{17}O as in SDPF-M. The adjusted SPEs are $\epsilon_{d_{5/2}} = 8.01$ MeV, $\epsilon_{d_{3/2}} = 10.11$ MeV, and $\epsilon_{s_{1/2}} = 2.11$ MeV. The p-shell SPEs are obtained based on SFO but with slight changes by fitting the ground-state energies of the studied nuclei and related levels such as the $1/2^-_1$ state in ^{11}B and $3/2^-_1$ state in ^{13}C. We obtain $\epsilon_{p_{3/2}} = 1.05$ MeV and $\epsilon_{p_{1/2}} = 5.30$ MeV. The detailed TBME of the present Hamiltonian can be obtained by contacting the authors.

We compare the TBME of the present Hamiltonian with those of WBT and WBP in Fig. 1. The TBME of central, spin-orbit and tensor interactions are also presented by the spin-tensor decomposition method [16]. The sd and $ppsdsd$ parts of WBT and WBP are the same between the two. So we show only the WBT result in these two parts. The sd part of the present interaction is from SDPF-M which is modified from USD (the same as the sd part of WBT) interaction. There is not much difference between WBT and the present interaction in the sd part. In the p part, all three of these interactions (i.e., the present interaction and the WBT and WBP interactions) are fit

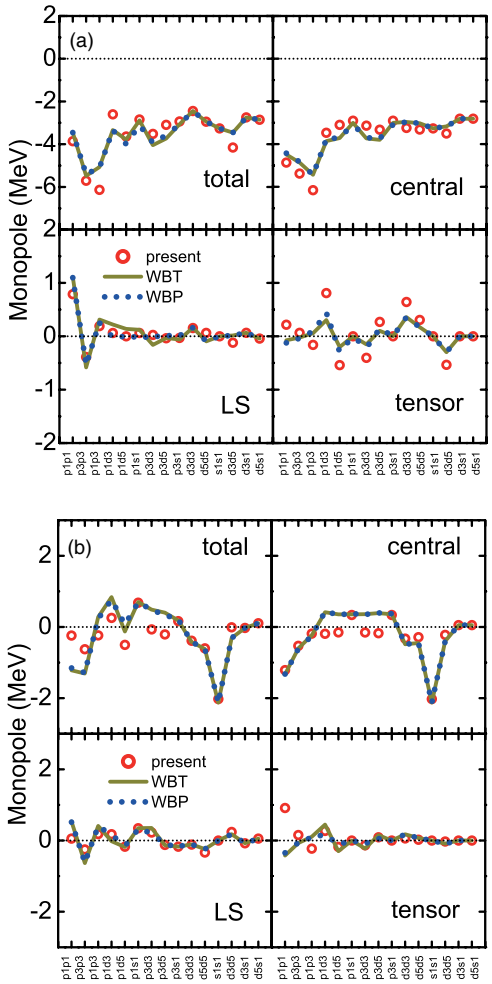

FIG. 2. (Color online) Monopole terms of total, central, spin-orbit, and tensor forces in each isospin channel: (a) $T = 0$ and (b) $T = 1$.

to low-lying levels of the p-shell nuclei. The difference among these three interactions is not large except for the tensor force. In the psd and $ppsdsd$ parts of the interaction, the deviation of the present interaction from WBT (WBP) turns out to be larger. The central force of the present interaction in the psd part is $0.85V_{MU}$. We find that this strength is proper because the number of points above the diagonal line is close to that below the line, as shown in the Fig. 1(c). It is interesting that the spin-orbit interaction of the present interaction is very similar to that of the WBP interaction in both the psd and $ppsdsd$ parts. In these two parts of the interaction, WBP has 10 parameters for the potential fitting while the present interaction is taken from the M3Y potential. Quite similar results between WBP and the present interaction indicate that the spin-orbit force is rather well determined compared to the central force.

Figure 2 presents the monopole terms of the interactions and their spin-tensor components. The monopole term is a weighted average of TBME for orbits j and j' [17,18]:

$$V^T_{j,j'} = \frac{\sum_J (2J+1)\langle jj'|V|jj'\rangle_{J,T}}{\sum_J (2J+1)}. \tag{4}$$

The monopole terms are presented in three groups, pp, $sdsd$, and psd in each picture. In each group the central monopole is relatively flat compared with the total monopole. The total interaction can be recognized as a global central force plus other staggers. The $T = 0$ central monopole is the most attractive among all these six central, spin-orbit, and tensor monopoles. The nuclear binding energy comes mostly from this interaction. Both $T = 0$ and $T = 1$ spin-orbit monopoles of the present interaction are very close to those of WBP. This is consistent with the analysis of the spin-orbit part of the TBME. Comparing with WBT, the present spin-orbit monopoles are also not much different. The present tensor force is stronger than WBT and WBP in the $T = 0$ channel, more attractive in $\langle p_{1/2}d_{5/2}|V|p_{1/2}d_{5/2}\rangle$, and more repulsive in $\langle p_{3/2}d_{5/2}|V|p_{3/2}d_{5/2}\rangle$. In the sd region of nuclei, this effect of the tensor force is canceled as the $p_{1/2}$ and $p_{3/2}$ orbits are fully occupied [19]. Going to the psd region, such as neutron-rich boron, carbon, and nitrogen isotopes, the opposite sign of the monopoles of the tensor force turns out to be important.

III. COULOMB CORRECTION

In the shell-model study, Coulomb interaction is not included in many cases in order to keep the isospin symmetry. When we compare the ground-state energies between theoretical results and observed values, Coulomb correction is needed. Present calculations in psd model space do not include the ground-state energies of ^{4}He, $E(^4He)$, which also needs to be removed. The total correction is

$$E_{\text{correction}} = E_{\text{expt.}} - E_{\text{Coulomb}} - E(^4He), \tag{5}$$

where E_{Coulomb} and $E_{\text{correction}}$ are the energy of the Coulomb correction and the ground-state energy after the correction, respectively. $E(^4He) = -28.296$ MeV. E_{Coulomb} is calculated through a similar method used in the construction of the WBT and WBP interactions [7]. We calculate the energy difference of mirror nuclei near $N = Z$ where the observed ground-state energies are taken from Ref. [20]. This E_{Coulomb} depends only on Z in our calculation. $E_{\text{Coulomb}} = 1.075$ ($Z = 3$), 2.720 ($Z = 4$), 4.593 ($Z = 5$), 7.368 ($Z = 6$), 10.248 ($Z = 7$), 13.854 ($Z = 8$) MeV.

IV. CENTER-OF-MASS CORRECTION

Because our calculation is done in two major shells, we need the center-of-mass (c.m.) correction to remove the spurious components which come from the c.m. motion. We use the method suggested by Gloeckner and Lawson [21]. In the calculations, the Hamiltonian is $H' = H_{SM} + \beta H_{\text{c.m.}}$, where H_{SM} and $H_{\text{c.m.}}$ are the original and c.m. Hamiltonians, respectively. If β is large enough, the effect of the c.m. motion is small enough in low-lying states. Figure 3 indicates some physical quantities of ^{16}C to check whether this method works or not, and how large a β is needed.

We find that the number of nucleons in the sd shell, $B(E2; 0^+_1 \to 2^+_1)$, or the energy of 2^+_1 in ^{16}C hardly change when β changes. The ground-state energy of ^{16}C changes quickly when β is small. For $\beta > 10$, it becomes almost flat. We use $\beta = 10$ in the following calculations.

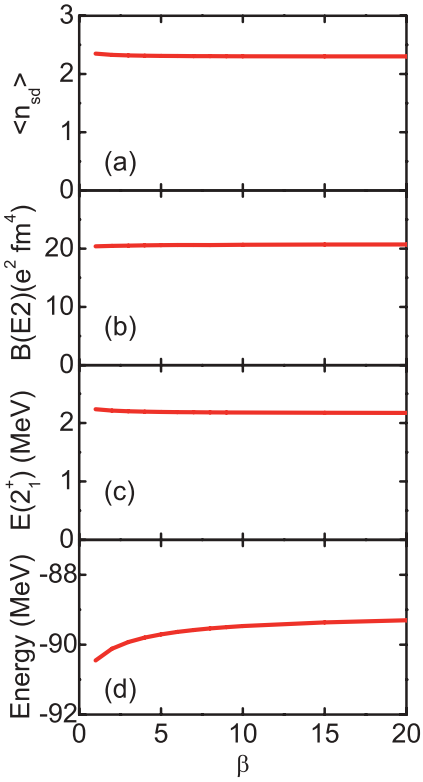

FIG. 3. (Color online) Effects of the center-of-mass corrections in four physical quantities: (a) nucleon number in *sd* shell, (b) $B(E2;0_1^+ \rightarrow 2_1^+)$ value, (c) $E(2_1^+)$, and (d) ground-state energy of ^{16}C. Their values change as the function of β.

V. GROUND-STATE ENERGY AND ENERGY LEVEL

The nuclei ^{22}C, ^{23}N, and ^{24}O are the last bound nuclei in neutron-rich side of C, N, and O isotopes [22]. The neutron-drip lines in elements beyond oxygen is not determined yet [22]. In WBT and WBP, ^{22}C is unbound and ^{26}O is bound. The present Hamiltonian improves the description of the drip lines of C and O isotopes. Figures 4 to 6 present the ground-state energies as well as one- and two-neutron separation energies S_n and S_{2n}, for B, C, N, and O isotopes. For O isotopes, the

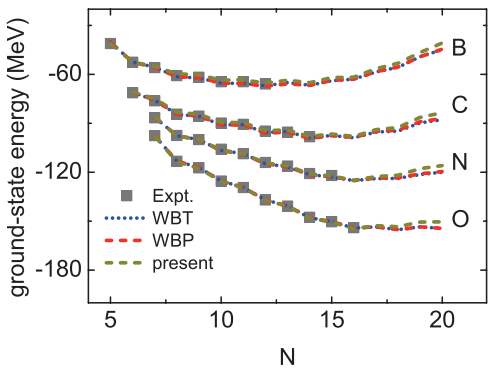

FIG. 4. (Color online) Ground-state energies of boron, carbon, nitrogen, and oxygen isotopes. Experimental values are taken from Ref. [20].

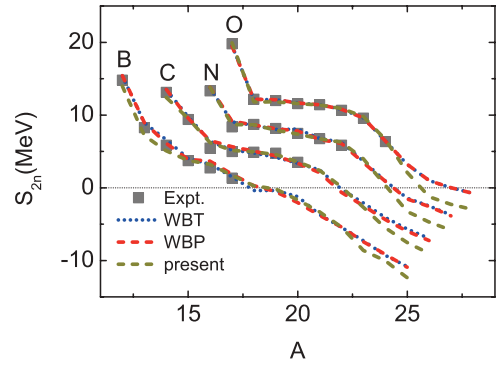

FIG. 5. (Color online) Two-neutron separation energies, S_{2n}, of boron, carbon, nitrogen, and oxygen isotopes. Experimental values are taken from Ref. [20].

WBT and WBP interactions have the same result as their *sd* parts. From S_n and S_{2n} of O isotopes, one can see that both WBT and the present Hamiltonian predict ^{25}O to be unbound, which is consistent with experiment [22]. ^{26}O is about 1.2 MeV unbound in the present result and 1.0 MeV bound in WBT. The positive S_n value in ^{26}O indicates that ^{26}O is one-neutron bound but two-neutron unbound. In N isotopes, all these three interactions can reproduce that ^{23}N is bound and ^{24}N and ^{25}N are unbound. ^{21}C is unbound experimentally [22] and also unbound in the calculations by all three of these interactions. ^{22}C is 0.1 MeV bound in the present result and 0.2 and 0.6 MeV unbound in WBT and WBP, respectively. ^{16}B is 40 (60) keV unbound [20]. It is 144 keV bound in WBP and 65 and 153 keV

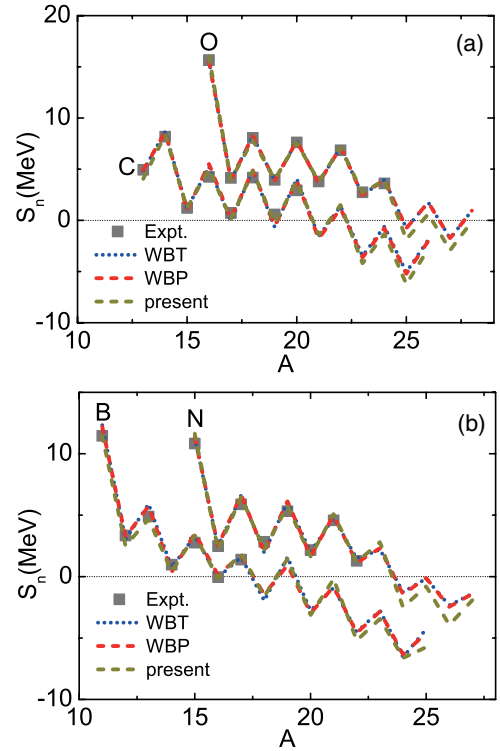

FIG. 6. (Color online) One-neutron separation energies, S_n of boron, carbon, nitrogen, and oxygen isotopes. Experimental values are taken from Ref. [20].

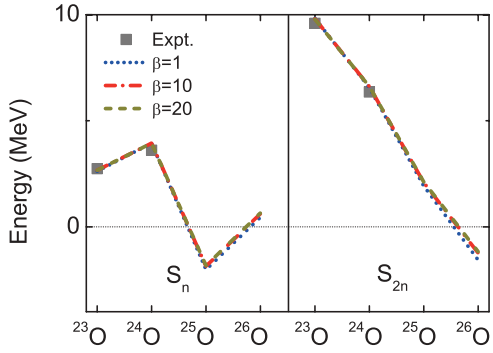

FIG. 7. (Color online) Comparison of S_n and S_{2n} under three different values of the center-of-mass parameter: $\beta = 1$, 10, and 20.

unbound in WBT and the present Hamiltonian, respectively. All Hamiltonians succeed in describing unbound ^{18}B. In the experiment [22], WBP, and the present Hamiltonian, it is one-neutron unbound. But in WBT it is both one- and two-neutron unbound. ^{19}B, which is experimentally bound [22], is unbound with 160, 381, and 538 keV in the present Hamiltonian, WBT, and WBP, respectively.

Here we briefly summarize the descriptions of drip lines by these three Hamiltonians. The present Hamiltonian is successful in describing all drip-line nuclei except for ^{19}B while WBT fails in ^{26}O, ^{22}C, ^{18}B, and ^{19}B and WBP fails in ^{26}O, ^{22}C, ^{16}B, and ^{19}B. One reason that the present interaction improves the description of drip lines is the inclusion of the mixing between $0\hbar\omega$ and $2\hbar\omega$ configurations. WBT and WBP have mass-dependent term in the *sd* shell [7]. Going from ^{18}O to ^{28}O, the *sd*-shell interaction decreases, which makes the nuclei less binding. We find that the mixing between $0\hbar\omega$ and $2\hbar\omega$ states has a similar effect. The partial effect of mass dependence therefore comes from the mixing between $0\hbar\omega$ and $2\hbar\omega$ states, which is not included in WBT and WBP. We will discuss more about the contribution of $2\hbar\omega$ states later.

In order to see if the prediction for the neutron drip line is sensitive to the center-of-mass parameter β, we have made calculations assuming three different values of the parameter. Figure 7 displays the calculations of one- and two-neutron separation energies under different β values, showing that

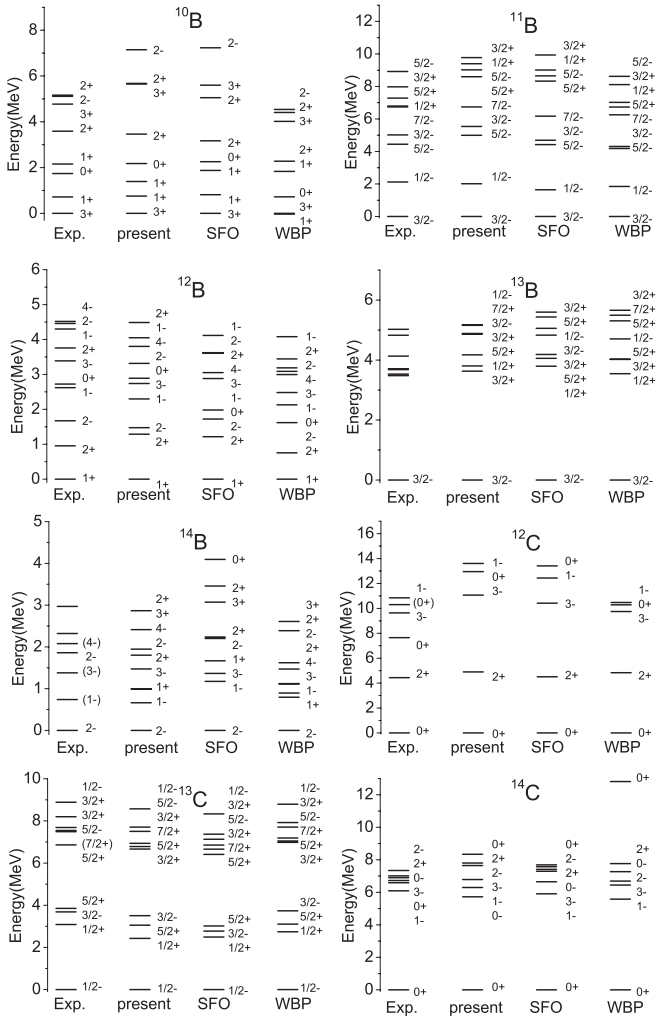

FIG. 8. Energy levels for boron and light carbon isotopes, obtained in the present, SFO, and WBP calculations, compared with experimental data [25–30].

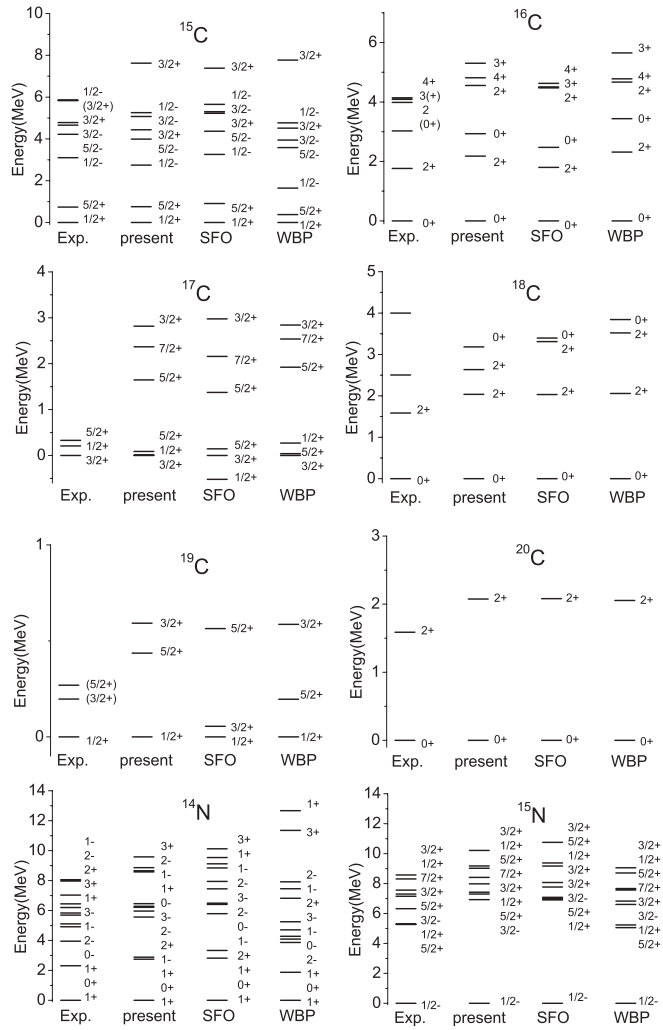

FIG. 9. Similar to Fig. 8, but for heavier carbon and light nitrogen isotopes.

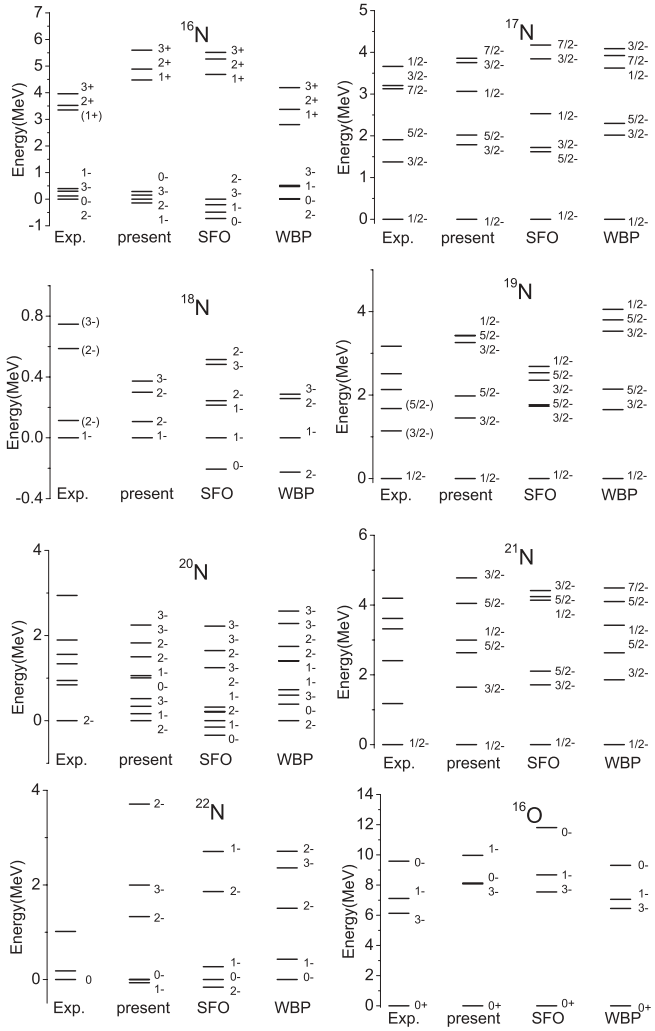

FIG. 10. Similar to Fig. 8, but for heavier nitrogen and light oxygen isotopes.

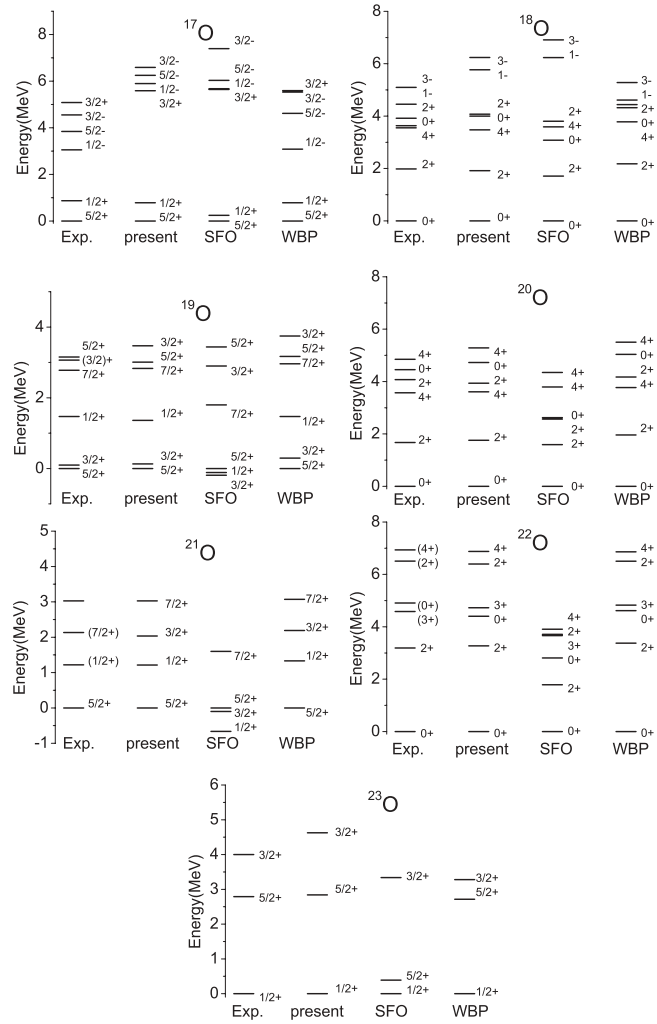

FIG. 11. Similar to Fig. 8, but for heavier oxygen isotopes.

the value of $\beta = 10$ used in the present work is large enough to remove the spurious center-of-mass components. For example, the neutron separation energies of neutron-rich oxygen isotopes change about 100 keV when increasing β from 1 to 10, while the separation-energy variation is about 20 keV when increasing β from 10 to 20. It is consistent with discussions in Sec. IV that the physical properties are well convergent when $\beta = 10$.

Figures 8 to 11 present the energy levels of B, C, N, and O isotopes. The agreement between experiment and the present work is fairly good. In particular, for ^{10}B and ^{18}N, we can reproduce the spins of the ground states of these two nuclei while WBP and WBT fail. WBT also fails in describing the spins of the ground states of ^{17}C, ^{19}C, and ^{16}N. We only show WBP results here because WBP is similar to WBT and is better in describing the spins of the ground states. The ground states of ^{16}N and ^{22}N are about 100 keV higher in the present interaction. The SFO can also reproduce the spin of the ground state of ^{10}B and nuclei nearby. But it fails in some neutron-rich nuclei such as ^{19}O and ^{21}O. This is because the $\langle sdsd|V|sdsd\rangle$ part of SFO is from the renormalized G matrix [8]. The interaction is too attractive without the contribution of three-body forces [2]. The first $1/2^+$ and $5/2^+$ states in ^{19}O, ^{21}O, and ^{23}O indicate that the neutron $1s_{1/2}$ orbit is too low compared with the neutron $0d_{5/2}$ orbit in SFO. This situation can be improved by using effective interactions such as SDPF-M or including the contribution of three-body forces [2], for instance.

The energy difference between the first 3^+ and 1^+ in ^{10}B can be reproduced well by both SFO and the present Hamiltonian. This is partly because the $0p_{1/2}$ orbit is much higher than the $0p_{3/2}$ orbit and partly because the strength of $\langle pp|V|sdsd\rangle$ is chosen properly, which will be discussed later. For ^{10}B and ^{11}B, an *ab initio* no-core shell-model calculation based on chiral perturbation theory showed that the inclusion of the three-body force is necessary to reproduce the ground-state spins [23]. In the present Hamiltonian, the phenomenological effective two-body interaction is mostly obtained by fitting experimental data. Therefore, the effective interaction thus obtained includes, at least partly, the three-body effect. Our calculations show this equivalence. In Ref. [2], it was pointed out that the *ab initio* interaction without three-body force cannot reproduce the neutron drip line of oxygen isotopes, while

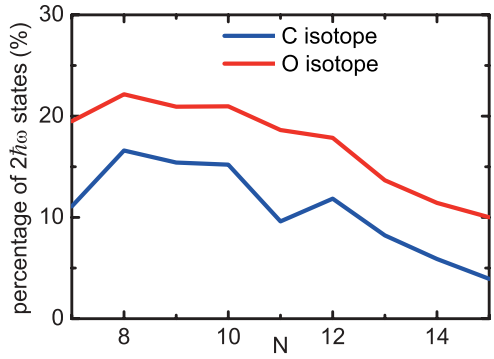

FIG. 12. (Color online) Percentage of $2\hbar\omega$ components in carbon and oxygen isotopes.

ab initio interaction with three-body force or phenomenological two-body interactions may describe the drip line.

The $\nu(sd)^3$ configuration shows different structure in $N = 11$ isotones from ^{17}C to ^{19}O [24]. $\nu(0d_{5/2})^3$ can couple to $J = 5/2$ with seniority $v = 1$ or couple to $J = 3/2$ with seniority $v = 3$. The structure of $\nu(sd)^3$ as well as the low-lying states in $N = 11$ isotones is a subtle problem because of these two configurations together with $\nu(0d_{5/2})^2(1s_{1/2})^1$, $\nu(0d_{5/2})^1(1s_{1/2})^2$, and many small components. For the first time, the present Hamiltonian in the full *psd* model space reproduces the low-lying states in all three of these nuclei, ^{17}C, ^{18}N, and ^{19}O. The $\langle(0d_{5/2})^2|V|(0d_{5/2})^2\rangle_{J=0,T=1}$ paring interaction contributes to this good agreement because this paring is reduced in SDPF-M, which will make the $v = 1$ state less bound and keep the $v = 3$ state unchanged. As one can see, the 2^+ state in ^{18}N and the $5/2^+$ states in ^{19}O and ^{17}C in the present results become higher compared with those in WBP results. Other matrix elements also contribute to this subtle problem. We will discuss the contribution of $\langle pp|V|sdsd\rangle$ in ^{17}C later.

The WBP and WBT results show more expanded energy levels compared with observed energy levels in C and N isotopes [25,26]. This can be improved by reducing neutron-neutron interactions by 25% (for C isotopes) or 12.5% (for N isotopes) in the *sd* shell in WBP and WBT [25,26]. The spectra of the present interaction are not so expanded as in WBP and WBT for C, N, and O isotopes.

In the present work, energy levels of unnatural parity state are not fully considered. One reason is that experimental data of these energy levels are not very available in neutron-rich nuclei. Another reason is that the dimension of the calculation increases quickly when including $3\hbar\omega$ components. We can improve the description of these unnatural-parity states with more experimental data and more advanced computers in the future.

The strength of the interaction in the $\langle pp|V|sdsd\rangle$ matrix elements is not determined in PSDMK, WBP, and WBT and is not fully considered in SFO. In the present interaction, the strength of the central part of $\langle pp|V|sdsd\rangle$ is 55% of V_{MU}. We will show some examples that the $\langle pp|V|sdsd\rangle$ matrix elements are important in describing the nuclei being studied. The total wave function of a nucleus can be written as $\Psi = a\Psi(0\hbar\omega) + b\Psi(2\hbar\omega)$. Figure 12 shows the probability

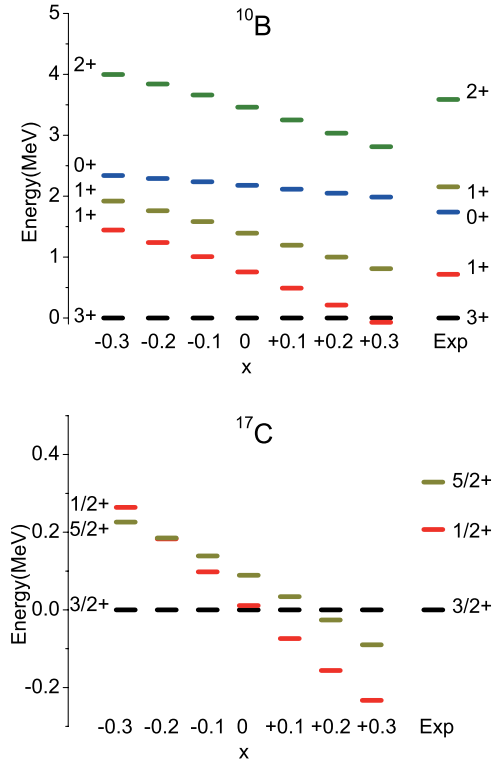

FIG. 13. (Color online) Energy levels of ^{10}B and ^{17}C as a function of x, which specifies the strength of the central force, $\langle pp|V|sdsd\rangle(\text{central}) = (0.55 + x)V_{MU}(\text{central})$.

b^2 of the $2\hbar\omega$ component. It is clear that the probability b^2 is very sensitive to neutron numbers. When the neutron number increases from 8 to 15, the value of b^2 decreases except for a singular point: ^{17}C. In WBP and WBT, the *sd* part includes the mass-dependent term $(18/A)^{1/3}$ [7]. Only, with this effect, WBP and WBT can well reproduce the ground-state energies of these nuclei. The mass-dependent term is needed for calculations of nuclei in a large mass range because the nuclear force is related to the radii of nuclei as well as the nucleon number A. But in a range of nuclei with small mass numbers, the effect of mass dependence is not obvious when we include $2\hbar\omega$ components. In the present Hamiltonian, we can reproduce well the ground-state energies, separation energies, and energy levels of B, C, N, and O isotopes without a mass-dependent term. One can see from Fig. 12 that the inclusion of $2\hbar\omega$ components will automatically contain a part of the mass-dependent effects. More work is needed to study the mass-dependent effects in light nuclei.

The $\langle pp|V|sdsd\rangle$ matrix elements are also important for energy levels in certain nuclei. Figure 13 shows the dependence of the energy levels in ^{10}B and ^{17}C on the interaction. Energy differences, such as difference between 3_1^+ and 1_1^+ in ^{10}B and that between $3/2_1^+$ and $5/2_1^+$ in ^{17}C, are very sensitive to the strength of $\langle pp|V|sdsd\rangle$. The energy difference between 3_1^+ and 0_1^+ in ^{10}B, on the other hand, is hardly changed when the strength of the central part of $\langle pp|V|sdsd\rangle$ is changed by 60% of V_{MU}. The above observations suggest that the contribution of $2\hbar\omega$ components is not only A dependent but is also state dependent. The $2\hbar\omega$ components are 4.3%, 16.0%, and 6.0%

in the 3_1^+, 1_1^+, and 0_1^+ states in ^{10}B, respectively. It is interesting to do a systematic investigation on how $\langle pp|V|sdsd\rangle$ as well as $2\hbar\omega$ or more $\hbar\omega$ components affect the energies and effective operators, such as effective charges and spin g factors which will be mentioned in the next two sections.

VI. ELECTRIC QUADRUPOLE PROPERTIES

The present Hamiltonian has been shown to describe the energies of the psd-shell nuclei quite well. It is necessary to investigate whether this interaction gives appropriate wave functions as well. In this section, we discuss the electric quadrupole properties with the use of the present Hamiltonian and WBP. In the shell model, effective charges are needed because of the polarization of the core, which is not included in the model space [31,32]. One set of effective charges, $e_p = 1.3$ and $e_n = 0.5$, is suitable for sd-shell nuclei [31], which means that both valence protons and neutrons are excited in the sd shell. For valence protons and/or neutrons located in the p shell in neutron-rich nuclei, this set of effective charges becomes invalid [33,40].

Figure 14 shows the quadrupole moments in B, C, and N isotopes and $B(E2)$ in Be and C isotopes with two sets of effective charges: one is Z, N dependent [33] and the other is independent of Z and N. Experimental values are taken from Refs. [34–41]. For the Z- and N-independent effective charges, we obtain them by fitting to quadrupole moments of these nuclei except for ^{18}N and ^{10}B. The quadrupole moment of ^{18}N is not exactly determined as there are two experimental values [34]. In case of ^{10}B, Z- or N-independent effective charges cannot describe well its quadrupole moment, as will be discussed later.

The Z and N independent effective charges obtained for the present Hamiltonian and WBP are $e_p = 1.26$, $e_n = 0.21$ and $e_p = 1.27$, $e_n = 0.23$, respectively. We also get the effective charges for the present Hamiltonian in $0\hbar\omega$ model space, $e_p = 1.25$ and $e_n = 0.25$. The inclusion of the $2\hbar\omega$ model space reduces the effective charges a little. Both of them underestimate the quadrupole moments in stable nuclei such as ^{10}B, ^{11}C, and ^{12}N and overestimate those of the nuclei somewhat far from the stability line such as ^{15}B and ^{17}B. This probably means that stable nuclei have stronger core

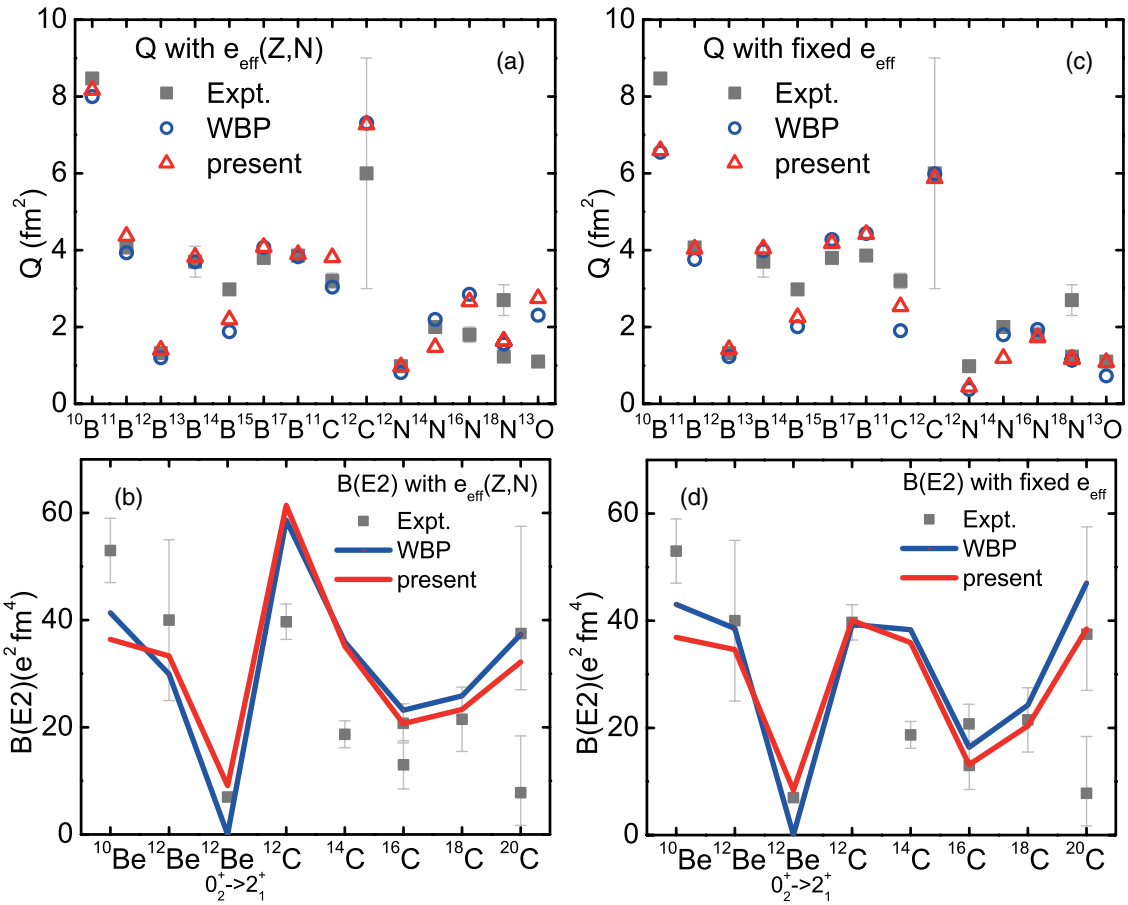

FIG. 14. (Color online) Electric quadrupole moments Q and $B(E2)$ values calculated by the present and WBP interactions and compared with experimental data [34–41]. Two sets of effective charges are used: one is Z, N dependent [33] and another is fixed to be $e_p = 1.26$, $e_n = 0.21$ and $e_p = 1.27$, $e_n = 0.23$ for the present and WBP interactions, respectively. (a) Electric quadrupole moments calculated with Z-, N-dependent effective charges. (b) $B(E2)$ values calculated with Z-, N-dependent effective charges. (c) Electric quadrupole moments calculated with fixed effective charges. (d) $B(E2)$ values calculated with fixed effective charges. All quadrupole moments are for the ground states except for 2_1^+ in ^{12}C. All $B(E2)$ values are from 0_1^+ to 2_1^+ except for the second $B(E2)$ value in ^{12}Be, which is from 0_2^+ to 2_1^+.

polarization while nuclei far from the stability-line have weaker core polarization. In nuclei far from the stability line, some valence nucleons are weakly bound, which will make the radial wave function extended farther than the well-bound nucleons. The extended wave function will reduce the interaction between valence nucleons and the core. In case of ^{12}C, the results for $B(E2)$ values with fixed effective charges are better than those with Z- and N-dependent effective charges. We emphasize that the smaller but constant effective charges can reproduce experimental data rather well in Fig. 14. The smallness may be explained as a consequence of the small core of ^{4}He in the present work. More studies on effective charges are of great interest.

Although none of the combinations of WBP or the present Hamiltonian with either set of effective charges works well in the quadrupole moment of ^{14}B, the present Hamiltonian improves the result of ^{14}B compared with WBP. We also calculate this quadrupole moment in the $0\hbar\omega$ model space with the present interaction. The result becomes worse than what we show in Fig. 14 which is obtained in the $2\hbar\omega$ model space. The ground state of ^{14}B includes 17% of $2\hbar\omega$ configurations. Including more $\hbar\omega$ excitations may improve the result of ^{14}B. The $2\hbar\omega$ configurations also improve the $B(E2;0_2^+ \rightarrow 2_1^+)$ of ^{12}Be. The 2_1^+ of ^{12}Be is almost a pure $2\hbar\omega$ state; that is, with 93% of the $2\hbar\omega$ components in the present Hamiltonian. The 0_1^+ and 0_2^+ of ^{12}Be have 64% and 54% of the $2\hbar\omega$ components, respectively. Therefore, although $B(E2;0_1^+ \rightarrow 2_1^+)$ values are very close to each other in WBP and the present results, they are contributed by different configurations in each calculation.

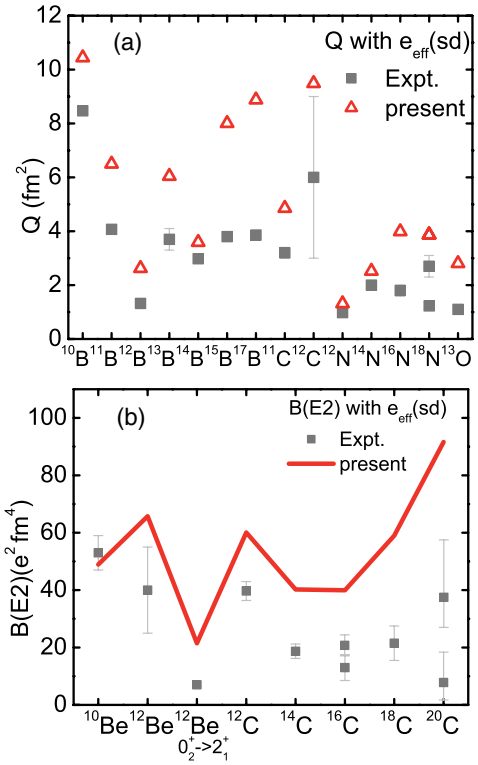

FIG. 15. (Color online) Similar to Fig. 14, but for $e_p = 1.3$ and $e_n = 0.5$.

In the WBP result, $B(E2;0_1^+ \rightarrow 2_1^+)$ of ^{12}Be is all from the contributions by the transition between p-shell nucleons, especially the transition inside the $0p_{3/2}$ proton orbit. In the present result, besides p-shell protons, p- and sd-shell neutrons contribute a lot to $B(E2;0_1^+ \rightarrow 2_1^+)$ in ^{12}Be. In ^{12}Be, the pure p-shell proton is not enough to reproduce the $B(E2;0_2^+ \rightarrow 2_1^+)$ value, as we see in Fig. 14.

We also try the conventional effective charges for the sd shell, $e_p = 1.3$ and $e_n = 0.5$, to calculate quadrupole moments and $B(E2)$ values with the present Hamiltonian (see Fig. 15). It is seen clearly that this set of effective charges is also invalid for this new Hamiltonian. Almost all values are much overestimated with this set of effective charge.

VII. SPIN PROPERTIES

If two protons (neutrons) couple to a pair of angular momentum zero, their total magnetic moment (m.m.) is zero. The m.m. reflects the motion of unpaired protons and/or neutrons. Figure 16 presents the m.m. with WBP and the present Hamiltonian in both $0\hbar\omega$ and $2\hbar\omega$ model spaces with $\delta g_{\pi,\nu}^{(l)} = \pm 0.1\mu_N$ and $g_s^{(\mathrm{eff})}/g_s = 0.95$, 0.92, and 0.90 for the present $2\hbar\omega$, the present $0\hbar\omega$, and WBP, respectively. $\delta g^{(l)}$ comes from the meson exchange processes [42,43] and $\delta g^{(s)}/g^{(s)}$ is obtained from the χ-square fitting of the calculated values to the experimental ones in these nuclei. All theoretical results reproduce well the observed values except

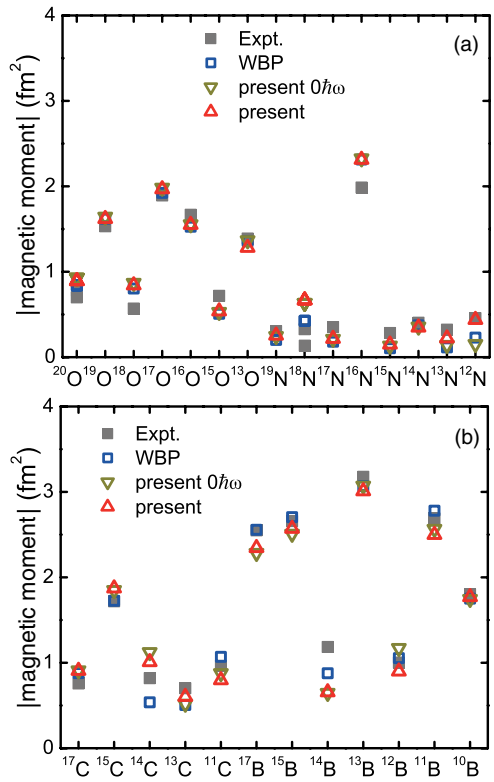

FIG. 16. (Color online) Magnetic moments calculated with WBP in $0\hbar\omega$, present in both $0\hbar\omega$ and $2\hbar\omega$ model spaces, compared with experimental data [34]. All magnetic moments are for the ground states except for 2_1^+ in ^{20}O and ^{18}O and 3_1^- in ^{16}O and ^{14}C.

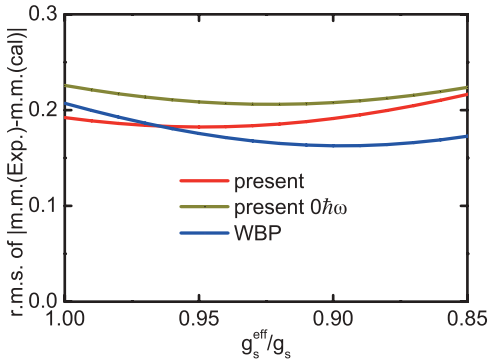

FIG. 17. (Color online) Root-mean-square deviation between calculated magnetic moments (m.m.) and the experimental ones, |m.m.(Expt.) − m.m.(Calc.)|, as a function of $g_s^{(\mathrm{eff})}/g_s$.

for a few nuclei. The largest deviation between calculations and experimental results is found in ^{18}O, ^{16}N, ^{14}C, and ^{14}B. Notice that their $E2$ properties are also not well described. We do not show the result for ^{18}O in the present work. Its calculated $B(E2)$ value is much smaller than the observed one. These nuclei may demand larger model space with $4\hbar\omega$ or more excitations.

In Fig. 17, we also show the root-mean-square (rms) deviation between calculations and observed values, |m.m.(Expt) − m.m.(Calc)|, versus $g_s^{(\mathrm{eff})}/g_s$. In a region $\delta g_s^{(\mathrm{eff})}/g_s = \pm 0.03$, the rms deviation of each result is very flat. Outside this region, the rms deviation increases. The minimal point for the rms deviation is located at $g_s^{(\mathrm{eff})}/g_s = 0.95, 0.92$ and 0.90 for the present $2\hbar\omega$, the present $0\hbar\omega$ and WBP, respectively. As we expect, the quenching is weaker when we enlarge the model space. The quenching of the present $2\hbar\omega$ result is rather weak and we may safely use bare g_s. If all results are with bare g_s, the present Hamiltonian gives the smallest rms deviation. We should also note, on the other hand, that the quenching factor obtained here has some ambiguity as the dependence of the rms deviation on the value of $g_s^{(\mathrm{eff})}/g_s$ is quite modest.

Table I presents the Gamow-Teller transition rates B(GT). The B(GT) values can be extracted from experimental log ft values with the equation

$$ft = \frac{6147}{(g_A/g_V)^2 B(\mathrm{GT})}, \tag{6}$$

where 6147 is from Ref. [44], and g_A and g_V are the axial-vector and vector coupling constants, respectively. For beta decays, we use bare $g_A/g_V = -1.26$ [45]. The calculated results are with $g_A^{(\mathrm{eff})}$ which is from χ-square fitting of these B(GT) values. $(g_A^{(\mathrm{eff})}/g_A) = 0.72$, 0.68, and 0.64 for the present $2\hbar\omega$, the present $0\hbar\omega$, and WBP, respectively. The $(g_A^{(\mathrm{eff})}/g_A)$ value for WBP is very close to the commonly used value 0.60 [31]. ^{11}Li and ^{15}C are weakly bound with 0.325 and 1.218 MeV neutron separation energy, respectively. The protons in their daughter nuclei from β decay are well bound. Halo or skin effects need to be included which is not included

TABLE I. B(GT) values of experiment, WBP, and present interaction for both $0\hbar\omega$ and $2\hbar\omega$ results. Experimental values are taken from Ref. [8] and related references in this paper.

Transition	$J_i^\pi T_i, J_f^\pi T_f$	Experiment	Present $2\hbar\omega$	Present $0\hbar\omega$	WBP
^{10}C→^{10}B	$0^+1, 1^+0$	3.467 (8)	3.256	2.724	3.022
^{11}C→^{11}B	$\frac{3}{2}^-\frac{1}{2}, \frac{3}{2}^-\frac{1}{2}$	0.3472 (45)	0.3606	0.3638	0.5043
^{11}Li→^{11}Be	$\frac{3}{2}^-\frac{5}{2}, \frac{1}{2}^-\frac{3}{2}$	0.0086 (24)	0.0079	0.0266	0.0126
^{12}Be→^{12}B	$0^+2, 1^+1$	0.624 (3)	0.754	1.488	1.359
^{12}N→^{12}C	$1^+1, 0^+0$	0.2950 (21)	0.2866	0.3650	0.3085
	$1^+1, 2^+0$	0.0273 (5)	0.0335	0.0405	0.0145
^{12}B→^{12}C	$1^+1, 0^+0$	0.3288 (15)	0.2866	0.3650	0.3085
	$1^+1, 2^+0$	0.0298 (10)	0.0335	0.0405	0.0145
^{13}N→^{13}C	$\frac{1}{2}^-\frac{1}{2}, \frac{1}{2}^-\frac{1}{2}$	0.1960 (38)	0.1958	0.1668	0.1537
^{13}B→^{13}C	$\frac{3}{2}^-\frac{3}{2}, \frac{1}{2}^-\frac{1}{2}$	0.3580 (50)	0.4005	0.4536	0.4175
	$\frac{3}{2}^-\frac{3}{2}, \frac{3}{2}^-\frac{1}{2}$	0.137 (15)	0.137	0.173	0.137
	$\frac{3}{2}^-\frac{3}{2}, \frac{5}{2}^-\frac{1}{2}$	0.0181 (43)	0.0166	0.0243	0.0015
^{13}O→^{13}N	$\frac{3}{2}^-\frac{3}{2}, \frac{1}{2}^-\frac{1}{2}$	0.3221 (83)	0.4005	0.4536	0.4175
	$\frac{3}{2}^-\frac{3}{2}, \frac{3}{2}^-\frac{1}{2}$	0.110 (26)	0.137	0.173	0.137
	$\frac{3}{2}^-\frac{3}{2}, \frac{5}{2}^-\frac{1}{2}$	0.0106 (71)	0.0166	0.0243	0.0015
^{14}B→^{14}C	$2^-2, 1^-1$	0.291 (40)	0.2580	0.2600	0.1960
	$2^-2, 3^-1$	0.038 (2)	0.025	0.034	0.022
^{14}C→^{14}N	$0^+1, 1^+0$	$3.46\ (3)\times10^{-7}$	0.0344	0.0450	0.0042
^{14}O→^{14}N	$0^+1, 1^+0$	$2.02\ (4)\times10^{-7}$	0.0344	0.0450	0.0042
	$0^+1, 1^+0$	2.818 (106)	2.942	2.990	2.905
^{15}C→^{15}N	$\frac{1}{2}^+\frac{3}{2}, \frac{1}{2}^+\frac{1}{2}$	0.2978 (42)	0.4524	0.4797	0.1046
	$\frac{1}{2}^+\frac{3}{2}, \frac{3}{2}^+\frac{1}{2}$	$4.91\ (56)\times10^{-4}$	0.0069	0.0125	0.0001
^{15}O→^{15}N	$\frac{1}{2}^-\frac{1}{2}, \frac{1}{2}^-\frac{1}{2}$	0.2490 (20)	0.2172	0.2266	0.2133

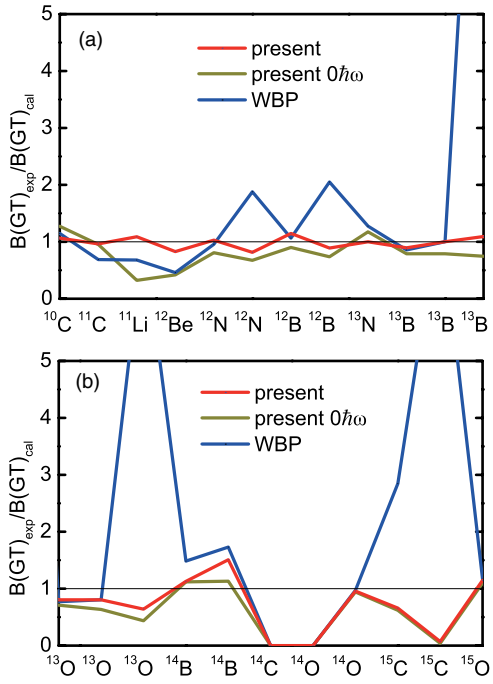

FIG. 18. (Color online) Ratio of the observed B(GT) values to calculated B(GT), $B(\mathrm{GT})_{\mathrm{expt}}/B(\mathrm{GT})_{\mathrm{calc}}$, in nuclei listed in Table I.

in calculations with harmonic oscillator bases. The overlap between related neutron and proton orbits is calculated in Woods-Saxon bases to modify the B(GT) of these two nuclei. All three of these calculated results (i.e., WBP and the present interaction in $2\hbar\omega$ and in $0\hbar\omega$) are modified by the halo or skin. More details can be found in Ref. [8].

The present $2\hbar\omega$ results improve most of the B(GT) values compared with the present $0\hbar\omega$ and WBP results. In order to show the difference between calculations and observed values, we present $B(\mathrm{GT})_{\mathrm{expt}}/B(\mathrm{GT})_{\mathrm{calc}}$ in Fig. 18. $B(\mathrm{GT})_{\mathrm{expt}}/B(\mathrm{GT})_{\mathrm{calc}}$ from the present $2\hbar\omega$ calculation is very close to unity except for ^{14}C and ^{14}O, and the second transitions in ^{15}C. ^{14}C and ^{14}O are the same in the present isospin symmetric Hamiltonian. The abnormally long lifetime of ^{14}C has been a long-standing theoretical problem [46]. The present $0\hbar\omega$ and WBP results also fail in describing B(GT) for ^{14}C and ^{14}O. The reason is that two main components of the transition almost all cancel in ^{14}C [46]. It is hard to describe the cancellation exactly in interactions determined by considering all nuclei nearby. In case of the the second transition from ^{15}C to ^{15}N, the reason is similar; that is, three components are canceled resulting in a rather small value.

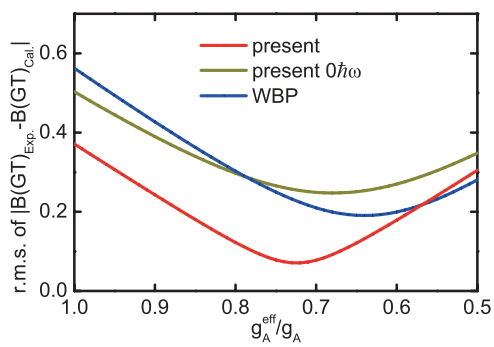

FIG. 19. (Color online) Root mean square of $|B(\mathrm{GT})_{\mathrm{calc}} - B(\mathrm{GT})_{\mathrm{expt}}|$ as a function of $g_A^{(\mathrm{eff})}/g_A$.

Similar to the discussion for m.m., the rms deviation of calculated B(GT) values from the experimental ones is presented in Fig. 19. It is clearly seen that both the rms deviation and the quenching get smaller when the model space is enlarged.

VIII. SUMMARY

In the present work, we present a systematic study of boron, carbon, nitrogen, and oxygen nuclei in full psd model-space with a newly constructed Hamiltonian. While some former Hamiltonians, such as PSDMK, WBP, and WBT, are constructed in $(0-1)\hbar\omega$ model space, we include $(2-3)\hbar\omega$ excitations in the present work. The present Hamiltonian is based on V_{MU} and has four parts, $\langle pp|V|pp\rangle$ from SFO, $\langle sdsd|V|sdsd\rangle$ from SDPF-M, $\langle psd|V|psd\rangle$ and $\langle pp|V|sdsd\rangle$ from V_{MU}, plus the spin-orbit force. We optimize the central part of V_{MU} while the tensor force in V_{MU} and the spin-orbit force are kept unchanged. The central force in $\langle psd|V|psd\rangle$ is 30% of V_{MU}s stronger than that in $\langle pp|V|sdsd\rangle$, while the strength of these two parts are the same in WBP. The SPE of the five orbits are also modified. More details on this Hamiltonian are explained in the text.

The present Hamiltonian can reproduce well the ground-state energies, drip lines, energy levels, electric properties, and spin properties of psd-shell nuclei. In particular, we can describe the drip lines of carbon and oxygen isotopes and spins of the ground states of ^{10}B and ^{18}N where WBP and WBT fail. The inclusion of $2\hbar\omega$ excitations is important in describing such properties because a part of the mass-dependent effect in WBP and WBT is naturally included when we include $2\hbar\omega$ excitations. The effective operators become closer, in general, to bare operators when we enlarge the model space. We note that constant and smaller effective charges work quite well in the present study, which may also be attributed to the small size of the ^{4}He core. The contribution coming from $2\hbar\omega$ excitations are investigated by comparison to $0\hbar\omega$ calculations, suggesting that the present model space is still insufficient to reduce effective charges almost to zero. More systematic study is needed in a model space larger than psd and more $\hbar\omega$ excitations, especially for $4p4h$ excitations from p to sd shells.

It is also examined whether the tensor force and the spin-orbit force can be kept unchanged in full shell-model calculations. Shell-model calculations without the modification of the strength of these two forces are found to be successful in the description of a wide range of psd-shell nuclei. It is interesting to do more work on applying the present tensor and spin-orbit forces to shell-model calculations in other region of nuclei.

ACKNOWLEDGMENTS

The shell-model calculations in this work are made by the codes OXBASH [47]. This work has been supported by the National Natural Science Foundation of China under

Grant No. 10975006. It has also been supported in part by Grants-in- Aid for Scientific Research (A) 20244022 and (C) 22540290 of the Ministry of Education, Culture, Sports, Science and Technology of Japan. The author C. Y. is grateful for the financial support from China Scholarship Council.

[1] R. V. F. Janssens, Nature (London) **459**, 1069 (2009).
[2] T. Otsuka, T. Suzuki, J. D. Holt, A. Schwenk, and Y. Akaishi, Phys. Rev. Lett. **105**, 032501 (2010).
[3] D. J. Dean, T. Engeland, M. Hjorth-Jensen, M. P. Kartamyshev, and E. Osnes, Prog. Part. Nucl. Phys. **53**, 419 (2004).
[4] T. Otsuka, T. Suzuki, M. Honma, Y. Utsuno, N. Tsunoda, K. Tsukiyama, and M. Hjorth-Jensen, Phys. Rev. Lett. **104**, 012501 (2010).
[5] N. Tsunoda, T. Otsuka, K. Tsukiyama, and M. Hjorth-Jensen, Phys. Rev. C **84**, 044322 (2011).
[6] D. J. Millener and D. Kurath, Nucl. Phys. A **255**, 315 (1975).
[7] E. K. Warburton and B. A. Brown, Phys. Rev. C **46**, 923 (1992).
[8] T. Suzuki, R. Fujimoto, and T. Otsuka, Phys. Rev. C **67**, 044302 (2003).
[9] T. Suzuki and T. Otsuka, Phys. Rev. C **78**, 061301(R) (2008).
[10] N. Tsunoda, K. Takayanagi, M. Hjorth-Jensen and T. Otsuka (unpublished).
[11] M. Hjorth-Jensen, T. T. S. Kuo, and E. Osnes, Phys. Rep. **261**, 125 (1995).
[12] S. K. Bogner, T. T. S. Kuo, and A. Schwenk, Phys. Rep. **386**, 1 (2003); S. K. Bogner, R. J. Furnstahl, S. Ramanan, and A. Schwenk, Nucl. Phys. A **784**, 79 (2007).
[13] G. Hagen, T. Papenbrock, D. J. Dean, A. Schwenk, A. Nogga, M. Włoch, and P. Piecuch, Phys. Rev. C **76**, 034302 (2007).
[14] Y. Utsuno, T. Otsuka, T. Mizusaki, and M. Honma, Phys. Rev. C **60**, 054315 (1999).
[15] G. Bertsch, J. Borysowicz, H. McManus, and W. G. Love, Nucl. Phys. A **284**, 399 (1977).
[16] M. W. Kirson, Phys. Lett. B **47**, 110 (1973); I. Kakkar and Y. R. Waghmare, Phys. Rev. C **2**, 1191 (1970); K. Klingenbeck, W. Knüpfer, M. G. Huber, and P. W. M. Glaudemans, *ibid.* **15**, 1483 (1977).
[17] R. Bansal and J. French, Phys. Lett. **11**, 145 (1964).
[18] A. Poves and A. Zuker, Phys. Rep. **70**, 235 (1981).
[19] T. Otsuka, T. Suzuki, R. Fujimoto, H. Grawe, and Y. Akaishi, Phys. Rev. Lett. **95**, 232502 (2005).
[20] G. Audi, A. H. Wapstra, and C. Thibault, Nucl. Phys. A **729**, 337 (2003).
[21] D. H. Gloeckner and R. D. Lawson, Phys. Lett. B **53**, 313 (1974).
[22] M. Thoennessen, At. Data Nucl. Data Tables **98**, 43 (2012).
[23] P. Navrátil, V. G. Gueorguiev, J. P. Vary, W. E. Ormand, and A. Nogga, Phys. Rev. Lett. **99**, 042501 (2007).
[24] M. Wiedeking *et al.*, Phys Rev. C **77**, 054305 (2008).
[25] M. Stanoiu *et al.*, Phys. Rev. C **78**, 034315 (2008).
[26] D. Sohler *et al.*, Phys. Rev. C **77**, 044303 (2008).
[27] [http://www.nndc.bnl.gov/nudat2/].
[28] M. J. Strongman *et al.*, Phys. Rev. C **80**, 021302(R) (2009).
[29] M. Stanoiu *et al.*, Phys. Rev. C **69**, 034312 (2004).
[30] A. Schiller *et al.*, Phys. Rev. Lett. **99**, 112501 (2007).
[31] B. A. Brown, Prog. Part. Nucl. Phys. **47**, 517 (2001).
[32] E. Caurier, G. Martínez-Pinedo, F. Nowacki, A. Poves, and A. P. Zuker, Rev. Mod. Phys. **77**, 427 (2005).
[33] H. Sagawa, X. R. Zhou, X. Z. Zhang, and T. Suzuki, Phys. Rev. C **70**, 054316 (2004).
[34] N. J. Stone, At. Data Nucl. Data Tables **90**, 75 (2005).
[35] S. Raman, C. W. Nestor Jr., and P. Tikkanen, At. Data Nucl. Data Tables **78**, 1 (2001)
[36] S. Shimoura *et al.*, Phys. Lett. B **654**, 87 (2007).
[37] N. Imai *et al.*, Phys. Lett. B **673**, 179 (2009).
[38] M. Wiedeking *et al.*, Phys. Rev. Lett. **100**, 152501 (2008).
[39] H. J. Ong *et al.*, Phys. Rev. C **78**, 014308 (2008).
[40] Z. Elekes *et al.*, Phys. Rev. C **79**, 011302 (2009).
[41] M. Petri *et al.*, Phys. Rev. Lett. **107**, 102501 (2011).
[42] A. Arima, K. Shimizu, W. Bentz, and H. Hyuga, Adv. Nucl. Phys. **18**, 1 (1986); A. Arima and H. Hyuga, in *Mesons in Nuclei*, edited by D. H. Wilkinson and M. Rho (North-Holland, Amsterdam, 1979), Vol. II, p. 683.
[43] I. S. Towner, Phys. Rep. **155**, 263 (1987); I. S. Towner and F. C. Khanna, Nucl. Phys. A **399**, 334 (1983).
[44] J. C. Hardy, I. S. Towner, V. T. Koslowsky, E. Hagberg, and H. Schmeing, Nucl. Phys. A **509**, 429 (1990).
[45] P. Bopp, D. Dubbers, L. Hornig, E. Klemt, J. Last, H. Schütze, S. J. Freedman, and O. Schärpf, Phys. Rev. Lett. **56**, 919 (1986); D. Dubbers, Nucl. Phys. A **527**, 239c (1991).
[46] I. Talmi, Adv. Nucl. Phys. **27**, 1 (2003).
[47] B. A. Brown, A. Etchegoyan, and W. D. M. Rae, OXBASH, *the Oxford, Buenos-Aires, Michigan State, Shell Model Program*, Michigan State University Cyclotron Laboratory Report No. 524 (1986).